Experimental Thermal and Fluid Science 102 (2019) 506–516

Contents lists available at ScienceDirect

Experimental Thermal and Fluid Science

journal homepage: www.elsevier.com/locate/etfs

Study of water wetting in oil-water flow in a small-scale annular flume

Taylor Gardner, Luciano D. Paolinelli*, Srdjan Nesic

Institute for Corrosion and Multiphase Technology, Department of Chemical & Biomolecular Engineering, Ohio University, Athens, OH 45701, USA

ARTICLE INFO

Keywords:
Annular flume
Oil-water flow
Phase wetting
Low-cost testing
Corrosion
Dispersed flow

ABSTRACT

Proper characterization of the phase wetting regime (water wet or oil wet) in two-phase oil-water flow can lead to optimized measures for pipe integrity management and save cost. In previous work it was demonstrated that not only the physicochemical properties of the produced oil and water have an important impact on flow patterns, but also the wettability of the pipe surface can favor or hamper the contact with water. Since the wettability of steel pipes can be altered by the chemical composition of the oil and water phases, and due to the wide diversity of the chemical composition of produced crude oils and water, as well as different chemicals injected in production systems (e.g., corrosion inhibitors, scale inhibitors, de-emulsifiers), it is important to perform phase wetting experiments in dynamic conditions using representative fluids and pipe material. This study presents an experimental assessment of the phase wetting regime of oil-water flow using a small-scale annular flume of 5 l capacity, which is advantageous as a potential testing tool for crude oil-water flows compared to regular multiphase flow loops. A model oil and brine were used as experimental fluids and three different materials (carbon steel, stainless steel and a polyester plastic) were used to analyze the effect of flume surface wettability on the phase wetting regime. The results indicate that the annular flume is a promising low-cost tool to test dynamic phase wetting and dispersed flow of petroleum-water systems qualitatively as well as quantitatively. Moreover, basic hydrodynamic assessment of the annular flume flow was performed to evaluate available criteria to predict the stability of fully dispersed flow.

1. Introduction

Two-phase flows of oil and water in pipes are usual in the oil and gas industry. Water containing impurities such as dissolved gases (i.e., CO_2 and H_2S) is commonly coproduced with oil when extracted from geologic reservoirs. The transportation of this water with liquid hydrocarbons can lead to internal corrosion of carbon steel pipes when the water phase is in contact with the pipe walls [1–3]. The contact of corrosive water with the pipe surface is referred to as water wetting [2,4]. In contrast, liquid hydrocarbons are not corrosive when in contact with metal surfaces during transportation (referred to as oil wetting) [4,5]. In (near) horizontal lines, water tends to occupy the pipe bottom due to its higher density with respect to the oil phase. At low flow velocity, there is a distinct interface between the two phases, resulting in a stratified flow regime. In oil-dominated flow, if sufficient turbulent velocity fluctuations are present in the oil phase, the water phase is disrupted into droplets that are entrained into the oil. In this case, the continuous oil phase keeps water droplets dispersed and suspended against gravity, yielding an oil-wet pipe surface.

Understanding phase wetting can help engineers in the oil and gas industry to improve pipeline integrity management by focusing corrosion control measurements on pipeline areas that are likely to experience water wetting and allowing future decisions to be made with more confidence. To address this point, several experimental studies were conducted to determine phase wetting regimes in oil-water pipe flow [2,4,6–10]. Furthermore, the modeling of the occurrence of water wetting has been attempted as reported in numerous publications [2,4,10–13].

Previous hydrodynamic models [14,15] describing the onset of stratification from a dispersion in liquid-liquid pipe flow have been found to be potentially useful in water wetting prediction [16]. These models assume that the flow is already dispersed and evaluate the balance between buoyancy forces and turbulent flow forces on dispersed phase droplets as criteria to determine the stability of the dispersed flow. Brauner [14] included an additional criterion, as suggested by Barnea [17], that determines the limit of excessive droplet deformation where fully dispersed flow would no longer be stable. The developed criteria account for the effect of the fluids flow rates, fluid properties (e.g., density, viscosity, interfacial tension), and pipe geometry (e.g., diameter and inclination). However, the effect of the

* Corresponding author at: Institute for Corrosion and Multiphase Technology, Department of Chemical & Biomolecular Engineering, Ohio University, 342 W. State Street, Athens OH 45701, USA.
E-mail address: paolinel@ohio.edu (L.D. Paolinelli).

https://doi.org/10.1016/j.expthermflusci.2018.12.010
Received 16 July 2018; Received in revised form 10 November 2018; Accepted 7 December 2018
Available online 08 December 2018
0894-1777/

Nomenclature

A_a	area of the top and bottom walls of the annular flume, m^2
A_i	area of the inner wall of the annular flume, m^2
A_o	area of the outer wall of the annular flume, m^2
C_i	constant that relates the bottom wall shear stress with the inner wall shear stress, dimensionless
C_o	constant that relates the bottom wall shear stress with the outer wall shear stress, dimensionless
c'	radius of the adhesion patch of the attached sessile droplet, m
d_{crit}	critical droplet diameter, m
d_{cb}	critical droplet diameter from buoyancy criterion, m
$d_{c\sigma}$	critical droplet diameter from deformation criterion, m
d_{max}	maximum droplet diameter, m
f	Fanning friction factor, dimensionless
f_{fl}	Fanning friction factor of the bottom wall of the flume, dimensionless
g	gravitational acceleration, m/s^2
H	height of the annular flume, m
h'	height of the attached sessile droplet, m
r	radial coordinate, m
R	mid radius of the annular flume, m
R_i	inner radius of the annular flume, m
R_o	outer radius of the annular flume, m
Ra	arithmetic surface roughness, m
Re_{fl}	Reynolds number of the mixture flow in the flume, dimensionless
Rz	average mean peak to valley distance of a roughness profile, m
r'	radius of the attached sessile droplet, m
t	tangential coordinate, m
T	torque input on the rotating top plate, Nm
U_c	mean velocity of the continuous phase, m/s
U_{fl}	average mixture velocity in the flume, m/s
U_t	mean tangential velocity of the rotating top plate, m/s
W	width of the annular flume, m
z	vertical coordinate, m

Greek letters

β	pipe inclination angle from the horizontal, rad
ε_d	volumetric fraction of dispersed phase, dimensionless
ϵ	energy dissipation rate per unit of mass of the continuous phase, W/kg
ϵ_{fl}	energy dissipation rate per unit of mass of the continuous phase in the flume, W/kg
θ	contact angle of the attached sessile droplet, radians
ρ_c	continuous phase density, kg/m^3
ρ_d	dispersed phase density, kg/m^3
ρ_m	mixture density, kg/m^3
μ_c	continuous phase viscosity, Pa s
μ_m	mixture viscosity, Pa s
σ	interfacial liquid-liquid tension, N/m
τ_{wb}	wall shear stress at the bottom wall of the flume, Pa
τ_{wi}	wall shear stress at the inner wall of the flume, Pa
τ_{wo}	wall shear stress at the outer wall of the flume, Pa
τ_{wt}	wall shear stress at the top wall of the flume, Pa
$\bar{\tau_{wb}}$	mean wall shear stress at the bottom wall of the flume, Pa
$\bar{\tau_{wi}}$	mean wall shear stress at the inner wall of the flume, Pa
$\bar{\tau_{wo}}$	mean wall shear stress at the outer wall of the flume, Pa
$\bar{\tau_{wt}}$	mean wall shear stress at the top wall of the flume, Pa
Ω	rotation velocity of the top plate, rad/s

interaction of the interface of both water and oil phases with the solid pipe surface, commonly described as surface wettability, is overlooked.

Surface wettability has been found to be an influential factor on flow patterns in oil-water pipe flow according to several experimental works performed in pipes of internal diameters (ID) from 0.012 m to 0.1 m and different wettability [10,18–22]. In general, the use of hydrophobic pipe surfaces (e.g., plastic pipes) favored the presence of the hydrocarbon phase in contact with the pipe surface as well as the development of oil-continuous flow patterns across wide ranges of operating conditions.

Regarding oil-water flow in carbon steel pipes, which are often the only economic option, Tang [9] studied phase wetting using different crude oils and a model oil in a 0.1 m ID flow loop containing a carbon steel section. He found that full entrainment of water into oil and an oil-wet regime were achieved at lower mixture flow velocities in crude oil-water flow with respect to mineral oil-water flow. It was suggested that these results were not only related to differences in the properties of the oils such as density, viscosity and interfacial tension, but also that the wettability change of the carbon steel pipe due to contact with crude oil (e.g., from hydrophilic to hydrophobic) could substantially contribute to observed phenomena. Most recently, Paolinelli et al. [10] used carbon steel and PVC pipes with the same 0.1 m ID, but differing wettability, to study the phase wetting and water layer thickness in oil-water flows. They found that the wettability of the carbon steel surface in the model oil-water system relied heavily on the fluid that was first in contact with the surface, and that this phenomenon altered significantly the dynamic phase wetting behavior in oil-water flow. It was also found that the onset of fully dispersed water-in-oil flow can differ significantly depending on the surface wettability (hydrophilic or hydrophobic) of the pipe. Moreover, different mechanisms for water segregation from dispersed flow were identified relating to the wettability of the pipe surface. For example, in hydrophilic pipes, water droplet deposition and spreading lead to the formation of water "streams" and water wetting. On the other hand, in hydrophobic pipes, droplet sticking and spreading at the pipe wall is unlikely to occur and water dropout happens at lower flow velocities where droplets accumulate and coalesce at the pipe bottom.

In summary, the wettability of carbon steel pipes transporting crude oil and water can significantly change the entrainment of the water phase into the oil phase; and, consequently, the phase wetting regime. In this respect, it has been found that the wettability of carbon steel can be changed from hydrophilic to hydrophobic by contact with crude oil due to the adsorption of naturally present compounds, e.g., aromatic hydrocarbons, nitrogen and sulfur containing compounds, and organic acids [23–25]. Since crude oil chemical composition can vary significantly from one region to another, and from well to well, the effect that it may have on carbon steel wettability is uncertain and would need to be tested for each particular case. It is worth mentioning that chemicals commonly added to the produced stream of crude oil and water, e.g., corrosion inhibitors, scale inhibitors and de-emulsifiers, may also have an effect on carbon steel wettability and also the oil-water interfacial tension, making the assessment of field situations even more complex. Wettability experiments, involving measuring water-in-oil contact angles, are difficult and often impossible due to the opaqueness of most of the crude oils. Moreover, even if the wettability of a carbon steel-crude oil combination is known in advance, its effect on the actual phase wetting regime (resulting in oil wetting or water wetting) would also need to be tested and confirmed.

A common practice used by research labs to experimentally investigate and quantify phase wetting regimes in oil-water flow is the use of flow loops. Although these studies have provided valuable insights into flow patterns and phase wetting regimes, flow loops have

many drawbacks [2,26]. Flow loops require large volumes of fluids (e.g., more than 10 gallons). On top of the high costs of operating with such volumes, obtaining large amounts of representative crude oil for testing purposes is impractical. Additionally, cleaning crude oil out of pipes, pumps, tanks and other common parts in flow loops is very difficult and requires large amounts of time and expensive chemicals; furthermore, this generates significant volumes of waste. Due to the aforementioned factors, the flow loop apparatus is unfeasible for rapid and affordable experimenting. This creates a necessity for a smaller-scale apparatus that can provide qualitative and quantitative information of phase wetting regime in oil-water flow at lower cost, e.g., less oil and brine volumes, simpler operation, reduced cleaning times, etc.

In this context, a small-scale apparatus with an annular flume can be an effective candidate for testing phase wetting in oil-water flow. An example is a rectangular cross-section annular flume with a rotating top that drives the flow by shear similar to Couette flow, with static bottom and lateral walls. A device with these features was first used in corrosion-related research to analyze the characteristics of the produced oil-water flows in order to determine its feasibility as a tool to represent flow in pipelines [27,28].

de Dood [27] used Computational Fluid Dynamics (CFD) and made experimental measurements (e.g., flow velocity) to characterize the annular flume flow. He reported that this type of flow had significant differences with respect to pipe flow; for example, secondary cross flow components. Ligthart [28] carried out experiments to assess the feasibility of using the annular flume as a small-scale experimental facility for determining pipe flow behavior of crude oil-water mixtures for corrosion assessment purposes. Although qualitative comparison of the behaviors of different crude oils was possible giving some insight for practical cases, he concluded that the annular flume showed several drawbacks that would probably prevent lab results to be fully translated to field situations.

The annular flume has been successfully used to make qualitative assessment of phase wetting in oil-water two-phase flow. Li [26] showed that critical mixture flow velocities for full water-in-oil entrainment measured in the annular flume for oils with different physicochemical properties showed variations with the water cut similar to the trends observed in large scale flow loop experiments. Subsequently, Li et al. [29] used the annular flume to determine qualitatively that full oil-water entrainment can be obtained at lower mixture flow velocities by adding corrosion inhibitors. This beneficial effect was related to a reduction in the oil-water interfacial tension, therefore making water entrainment more probable.

Although the aforementioned studies assessed how the water phase interacts with the oil phase, they did not consider the influence of the surface wettability (e.g., hydrophobic or hydrophilic) on dynamic phase wetting. Systematic studies in this respect are needed for a comprehensive characterization of the annular flume as a qualitative and quantitative tool for phase wetting testing of field fluids in dynamic conditions. The present work shows a systematic study of the effect of surface wettability on phase wetting regime in oil-dominated oil-water horizontal flow in a small-scale annular flume. Flow tests with bottom surfaces made of carbon steel, stainless steel and polyester (PET) were performed to characterize phase wetting of surfaces whose wettability spanned from hydrophilic to hydrophobic. Some discussion on the hydrodynamics of the annular flume and its impact on multiphase flow are also provided.

2. Experimental

2.1. Small-scale annular flume description and instrumentation

Phase wetting and water layer thickness measurements in oil-water flow were performed using a small-scale annular flume. A schematic layout of the annular flume is shown in Fig. 1. The apparatus has four main components: a static outer cylinder, a static inner cylinder, and a static bottom plate, all made of stainless steel; and a rotating top plate (carousel) made of PVC. The annular flume conduit, which rectangular cross-section is highlighted using dashed red lines, is formed by the bottom of the carousel and the bottom plate (height $H = 0.05$ m), and the inner wall (radius $R_i = 0.14$ m) and outer wall (radius $R_o = 0.21$ m). The carousel is coupled to a shaft connected to a gearbox reducer (not shown in Fig. 1), powered by a motor with an electronic controller that provides stable rotation speed (Ω) with an accuracy of 5%.

As mentioned above, the rotating top plate drives the flow in the annular flume by shear, resulting in oil and water main flow in the tangential direction (t) of the flume as indicated by the tangential velocity vector drawn in Fig. 2b and c. Due to the curvature of the conduit, the flow is also accelerated in the radial (r) and vertical directions (z) producing secondary cross flow in the direction indicated in Fig. 2b and c. Maximum cross flow components can be about 25–30% of the maximum tangential velocity [30]. When the oil phase flows on top of the water phase fast enough, the water surface is sheared and disrupted into droplets that can be entrained by the turbulent oil phase (Fig. 2b). If the mixture velocity is high enough, all the water mass is entrained and the bottom wall becomes fully oil wet (Fig. 2c). This is somewhat similar to the entrainment phenomena that occur in turbulent horizontal pipe flow [10]. However, the existence of secondary cross flow in the annular flume leads to some differences that will be discussed further below.

Phase wetting regime and thickness of developed water layers were measured using a concentric two-electrode high frequency (HF) impedance probe with an inner carbon steel electrode of 12.5 mm diameter ($2r_i$) and an outer stainless steel electrode of 25 mm diameter ($2r_o$) described in previous studies [8,10]. The probe was used flush-mounted at the bottom wall of the flume, specifically positioned at the mid radius (R) as indicated in Fig. 1. It was operated with an AC voltage of 10 mV rms and frequency of 100 kHz using a Gamry REF 600® potentiostat with a computer interface. The impedance was monitored continuously for each flow experiment using a sampling period of approximately 0.5 s. The occurrence of water layers in contact with the probe, and their thickness, were obtained from the measured impedance modulus and phase angle in relation to the theoretical response of the probe and the electrical conductivity of the water phase [8]. The probe detects water layers as thin as 0.003 mm on average. The measurement of water layer thickness has an uncertainty of less than 10% for thicknesses lower than 3 mm. For thickness values from 3 mm

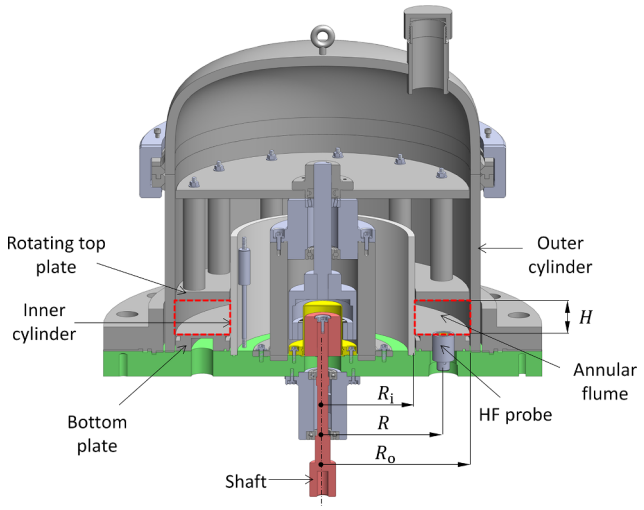

Fig. 1. Schematic of the apparatus used in the experiments with the annular flume highlighted using dashed red lines. (For interpretation of the references to colour in this figure legend, the reader is referred to the web version of this article.)

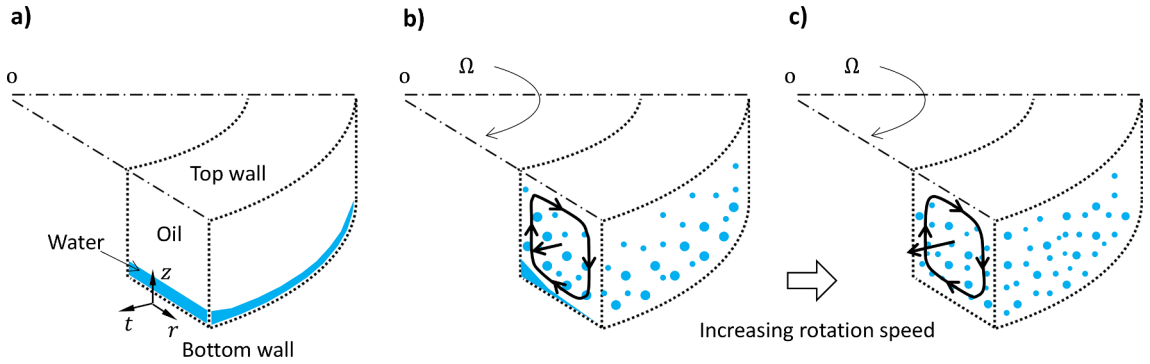

Fig. 2. Schematic representation of the oil-water flow in the annular flume. (a) Steady stratified regime; (b) semi-dispersed flow; (c) fully dispersed flow.

to 5 mm, the measurement uncertainty is about 15%.

Three types of bottom wall surfaces were tested: stainless steel, carbon steel and polyester (PET). The surface of the stainless steel bottom plate had arithmetic roughness (Ra) of 1.9 μm and average mean peak to valley distance (Rz) of 17 μm. The stainless steel bottom plate was coated with carbon steel foil or PET film to change the surface wettability when needed. The carbon steel surface was achieved by applying carbon steel foil of 0.05 mm thickness over the stainless steel bottom plate using liquid adhesive. The carbon steel foil was polished with 400 grit SiC paper to assure the same surface condition before each experiment. Surface roughness was measured as $Ra = 1.5$ μm and $Rz = 12$ μm. The plastic surface was obtained by applying auto-adhesive PET film of 0.05 mm thickness over the bottom plate. In this case, no surface polishing was required after applying the film due to its excellent surface quality ($Ra = 1$ μm and $Rz = 7$ μm), which remained unaltered.

Each flow experiment was performed using the following procedure: Before fluids were transferred into the flume, the leveling of the apparatus was checked. Due to its larger density, the desired amount of water was first carefully poured into the cell through a loading tube, followed by the oil until the level of the rotating top plate was reached. The total volume of fluids was 5.05 L. This amount was slightly larger than the ideal geometrical volume of the flume due to the gaps between the top and bottom plates and the outer and inner cylinders, and fitting openings located at the outer cylinder for eventual introduction of instrumentation (e.g., thermocouples, pitot tubes, etc.). The fluid mixture stayed at rest until the top plate was rotated. Phase wetting behavior at the bottom plate was constantly monitored by the flush-mounted HF impedance probe. The rotation speed started with a small value and then was gradually increased, incrementally, until the full oil wet regime was obtained at the bottom plate, due to complete entrainment of the water phase, or when the maximum allowable rotation speed of 135 rpm (mechanical limitation due to excessive vibration of the carousel) was reached. The rotation speed was increased in increments of 15–30 rpm. At every step, the rotation speed was kept constant for approximately 5 min, which is usually the time that it took to stabilize the phase wetting regime to its new state. Once the oil wet regime or the maximum allowable rotation speed was achieved, the rotation speed was slowly lowered until the system stopped. The flume was then drained and the oil-water mixture was separated by gravity in a large volume storage tank. The interfacial tension of the oil and water was measured before and after each the experiments to check if there were any changes. After complete separation of the oil and the water in the storage tank, the oil phase was reused for subsequent flow experiments and the water phase was discarded. Fresh brine was used as the water phase in each new flow experiment. After draining the fluids, thorough cleaning of the walls of the flume was performed using oil absorbent disposable cloths followed by rinses with isopropanol and deionized water, and drying with disposable clean cloths. The surface of the HF impedance probe was reconditioned by polishing with 400 grit SiC paper, washed with deionized water and isopropanol, dried with a flow of air, and flush mounted at the bottom plate for a new experiment. It is important to mention that ferric corrosion products formed on the carbon steel bottom surface during the experiments. In this case, the carbon steel surface was lightly polished with 400 grit SiC paper to remove corrosion products from the previous experiment and assure the same starting surface for the next experiment.

2.2. Experimental fluids and flow conditions

Two immiscible fluids were used for the flow experiments and the surface wettability measurements. The oil phase used was Isopar V®, a clear saturated paraffinic hydrocarbon. The water phase used was 1 wt % NaCl solution prepared from deionized water and granular NaCl (USP/FCC grade). The use of a highly conductive electrolyte as water phase (1.76 S/m) helps prevent significant local conductivity changes when the solution comes in contact with the flume bottom surface made of carbon steel, which can corrode and release iron ions.

The properties of the used fluids are listed in Table 1. The oil-water inversion point is the volumetric percent ratio of the water phase to the oil phase where a water-in-oil mixture spontaneously turns into an oil-in-water mixture. The oil-water inversion point was measured in a stirred vessel using high frequency conductance measurements with a parallel-rod two-electrode setup [10]. Flow experiments were performed at near room temperature (~25 °C) using rotation speeds from 17 to 135 rpm, which represents average mixture velocities in the flume from about 0.15 to 1.25 m/s. The used water/oil volumetric ratio, called herein the “water cut”, ranged from 2.5% to 20%. Water cuts below 2.5% were not tested due to the intrinsic difficulty of obtaining a continuous water layer covering the whole flat bottom surface of the flume as a starting point for the phase wetting measurements.

It is important to mention that the oil-water interfacial tension value shown in Table 1 corresponds to the interface between oil and fresh brine. This property was also measured after each flow experiment, and some changes were found depending on the type of bottom plate surface that was in contact with the water phase. This effect will be shown and discussed further below. The interfacial tension was measured using a Du Nouy tensiometer Kruss® K20 with a platinum ring.

Table 1
List of properties of the experimental fluids (values at 21 °C).

Property	Oil	Water
Density (kg/m^3)	805 ± 2	1005
Dynamic viscosity (Pa s)	0.01 ± 0.001	0.001
Oil-water interfacial tension (N/m) × 10^3	41.5 ± 1	
Oil-water inversion point (%)	25	

2.3. Wettability measurements

Static wettability measurements for each material used as the bottom surface of the annular flume were made using a goniometer with a digital image capturing system, described elsewhere [10]. Each specimen was immersed in 0.5 L of the hydrocarbon phase. An 8 μL droplet of the water phase was deposited on the immersed specimen's surface. The droplet Bond number based on its non-deposited radius was 0.06, which is low enough to avoid both shape distortion of the sessile droplet due to gravity and any error of measured contact angles [31]. The contact of droplets with the specimen's surface was monitored for up to 10 min.

Three kinds of specimens were tested. The first was a machined flat piece made of stainless steel, whose surface roughness matched that of the stainless steel bottom plate in the annular flume. The stainless steel specimen was tested under oil pre-wetted and water pre-wetted conditions. The second specimen was a flat stainless steel piece coated with the same carbon steel foil used on the bottom plate of the annular flume. The carbon steel surface was polished using the same procedure as in the flow experiment, and was also tested under oil pre-wetted and water pre-wetted conditions.

The oil pre-wetted condition consisted of cleaning the specimen surface with deionized water and isopropanol, then drying it using air current before being immersed in the hydrocarbon phase. The water pre-wetted condition consisted of immersing a clean specimen in the test water phase, then withdrawing it and flushing the surface with the hydrocarbon phase in an effort to thin the water film prior to the final immersion in the oil phase. The third specimen was another stainless steel piece coated with the same PET film as used in the flow experiment. In this case, the contact angle measurement was performed in oil-pre-wetted condition since the water phase did not remain at the plastic surface after contact.

ImageJ® software was utilized in analyzing each image of the droplets. The droplet height (h') and contact base ($2c'$) were measured. The contact angle was then estimated by the truncated sphere method:

$$\frac{c'}{h'} = \frac{\sin\theta}{1-\cos\theta} \tag{1}$$

where θ is the contact angle measured from inside of the deposited droplet as shown in Fig. 3.

3. Results and discussion

3.1. Wettability of the employed bottom plate surfaces

Fig. 4 shows the water-in-oil contact angle as a function of time measured on the carbon steel, stainless steel, and PET surfaces, all used in the bottom wall of the annular flume. The PET surface makes a contact angle of about 163 degrees with the droplet after the first seconds of contact. The contact angle decreases to about 130 degrees after 10 min showing a hydrophobic surface. Similarly, the oil pre-wetted stainless steel specimen shows hydrophobicity, making a contact angle of 161 degrees after the first seconds that decreases to 148 degrees after 10 min. In comparison, the water pre-wetted stainless steel specimen shows similar initial hydrophobicity, but the contact angle significantly decreases to about 107 degrees after 20 s. This value is close to the hydrophobic-to-hydrophilic transition limit (θ= 90°). This behavior is associated with the existence of water residues that remain attached in the valleys of surface roughness elements at the stainless steel surface, which favor the spreading of the contacting droplets.

The oil pre-wetted carbon steel surface shows hydrophobicity in the first seconds of contact. The contact angle then gradually decreases becoming hydrophilic after about 7 min, reaching a value of about 83 degrees after 10 min. In contrast, droplets on water pre-wetted carbon steel rapidly spread and collapse after about 3 s yielding a contact angle close to zero degrees, which denotes a high hydrophilicity. The wetting hysteresis seen on carbon steel is due to the surface's preferential adsorption of water molecules compared to oil. In a water-free oil pre-wetted carbon steel surface, the water phase takes some time to displace the hydrocarbon to reach its hydrophilic equilibrium, which may attain even lower contact angles than observed for 10 min at longer times. Nevertheless, when water first adsorbs on the carbon steel surface (water pre-wetting) a very thin water layer remains attached providing super hydrophilic characteristics. Similar behavior was observed on carbon steel specimens elsewhere [10].

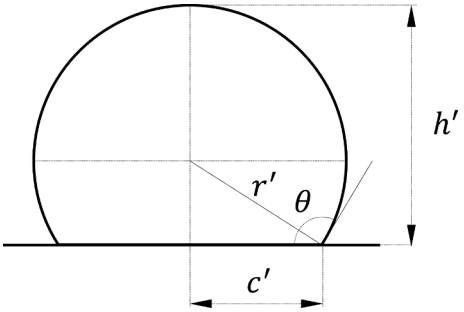

Fig. 3. Two-dimensional scheme of the sessile droplet geometry.

It is important to restate that loading the annular flume required the water phase to be poured in first, causing the surfaces to be water pre-wetted for each trial. Therefore, in the present model oil-brine system, carbon steel surfaces are expected to behave as super hydrophilic, and PET and stainless steel surfaces are expected to behave as hydrophobic. However, the latter may show some difference in water wetting due to the lower contact angles measured when the surface was pre-wetted with water.

3.2. Phase wetting and water layer thickness in oil-water flow in the annular flume with different bottom wall wettability

The flow experiments were performed for any given water cut by going from the lowest mixture velocity (0.15 m/s) and increasing it until the oil wet regime was consistently obtained or the maximum allowable rotation speed was reached. The average mixture flow velocity in the flume can be approximated as:

$$U_{\text{fl}} \cong \frac{U_t}{2} = \frac{\Omega R}{2} \tag{2}$$

where U_t is the mean tangential velocity of the rotating top plate, Ω is the rotation speed expressed in rad/s, and the mid radius of the flume is:

$$R = \frac{(R_o + R_i)}{2} \tag{3}$$

For this particular model oil-brine system, the mixture flow is expected to be turbulent at velocities above 0.18 m/s as will be discussed further below.

Fig. 5 shows the phase wetting regimes and time-averaged water layer thickness measured at the bottom plate for carbon steel, stainless steel and PET surfaces as a function of operating conditions (water cut and mixture velocity). The results are the average of at least 2 independent experiments with the same flow conditions. Reproducibility in terms of phase wetting regime and water layer thickness was good with differences less than 14% on average. The phase-wetting regimes are characterized as "full oil wet" (red[1] circles), where only oil was detected, or water wet where water was detected; the data is further

[1] For interpretation of color in Fig. 5, the reader is referred to the web version of this article.

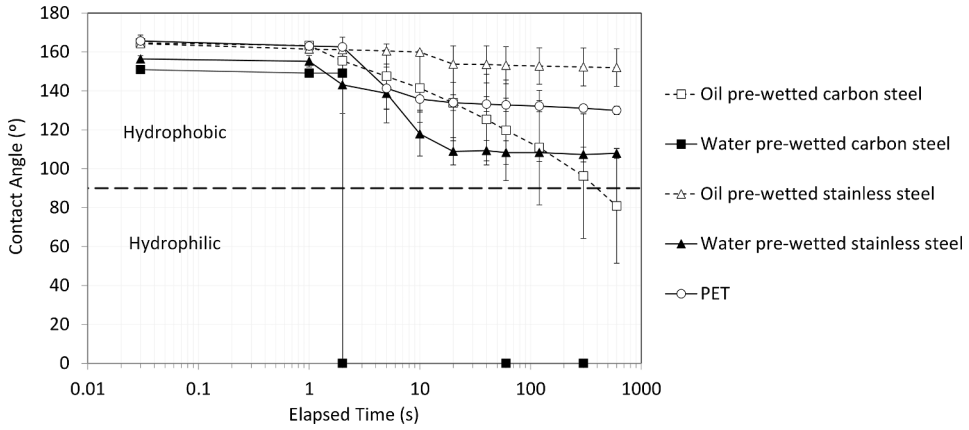

Fig. 4. Water-in-oil contact angle as a function of time for carbon steel, stainless steel, and PET surfaces.

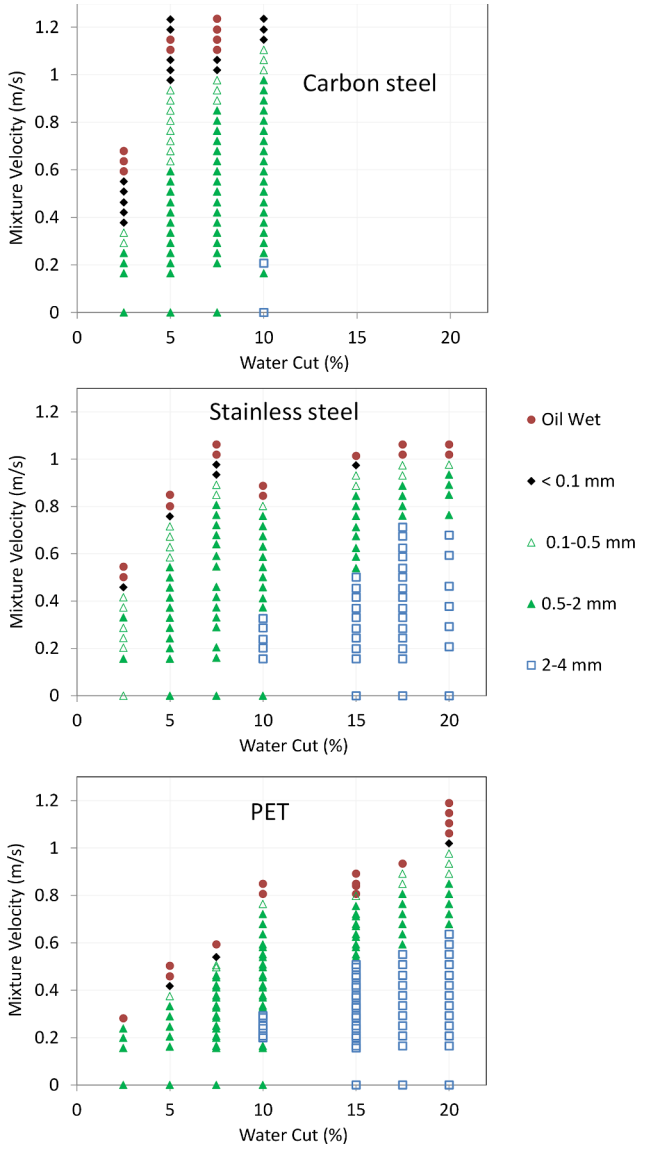

Fig. 5. Phase wetting regime and time-averaged water layer thickness at bottom plates with different wettability as a function of operating conditions in the annular flume oil-water flow.

arranged in ranges to illustrate the variation of water layer thickness (e.g., green triangles indicate average water layer thicknesses between 0.5 mm and 2 mm). The map for carbon steel surface shows no data for water cuts greater than 10% due to the fact that no full entrainment of water into oil could be seen. If the physical limitations of the equipment allowed for higher flow velocities, it would be possible to perform experiments with larger water cuts and achieve oil wet regime at the bottom of the flume.

In general, it was found that the higher the mixture velocity the smaller the water layer thickness, as expected. When the mixture velocity was high enough, the water was fully entrained leading to an oil-wet bottom surface. Fig. 6 shows the critical mixture velocities to obtain the oil wet regime. It is obvious that critical mixture velocities are significantly affected by the wettability of the bottom surface of the conduit. For the PET surface, mixture velocities of 0.4 m/s and 0.7 m/s are enough to obtain full oil wet regime for water cuts of 5% and 10%, respectively. On the other hand, the carbon steel surface needs significantly larger mixture velocities to attain full oil wet regime, i.e., 1 m/s for 5% water cut. It is interesting to note that full oil wet regime cannot be obtained in this case for the 10% water cut, even at the largest allowable mixture velocity of 1.25 m/s where very thin water layers (< 0.1 mm) are detected instead (Fig. 5 top). The stainless steel

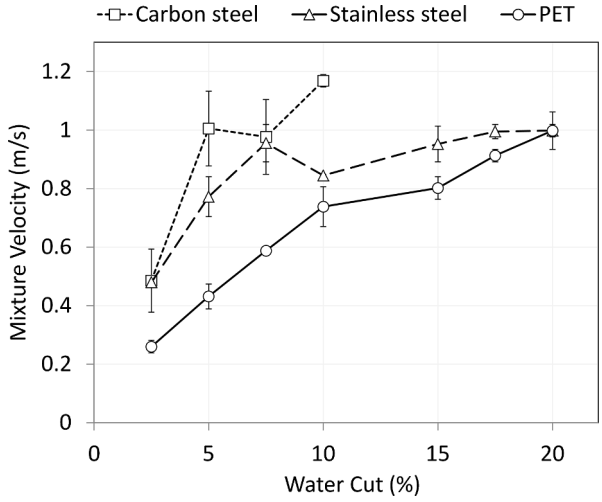

Fig. 6. Critical velocities for oil-wet regime measured for bottom plates with different wettability as a function of operating conditions in the annular flume oil-water flow.

surface requires mixture velocities larger than the PET but lower than the carbon steel to achieve the full oil wet regime for water cuts from 2.5% to 15%. However, the transition to oil wet regime is given at similar mixture velocities as the PET at larger water cuts.

The observed effect of the surface wettability of the annular flume on the critical mixture velocity to fully entrain the water phase, and achieve the full oil wet regime, is similar to what was found in previous work [10] performed in oil-water pipe flow in a large scale flow loop.

Irrespective of the material of the bottom surface and its wettability, in general the critical mixture velocity increases with the water cut. This is in line with the findings of Li et al. [29], who performed phase wetting measurements in oil-water flow in an annular flume of similar characteristics. The observed trend of larger critical mixture velocities for larger water cuts is also similar to what has been found in several studies in oil-water pipe flow focused on phase wetting [4,7,8,10], and also focused on flow patterns where fully dispersed water-in-oil regimes were studied [18,21,32].

Table 2 shows the oil-water interfacial tension (IFT) measured before and after each flow experiment. The IFT after the flow experiments is reported as the average minimum and maximum values measured in the entire set of different experiments performed for each bottom surface material. After the flow experiments using stainless steel and PET surfaces, the IFT showed a slight decrease from the initial value (i.e., < 17%). On the other hand, the IFT decreased up to about 35% after the flow experiments using a carbon steel surface. This effect may be related to the presence of relatively high concentrations of dissolved ferric ions in the brine (Table 3), which are products of the oxidation of the carbon steel surface. The hydrolysis of ferric ions reduces the pH of the brine, which may have some effect on the interfacial behavior between the brine and the model oil; particularly if any residual content of surfactants is present in the oil phase. As listed in Table 3, the content of dissolved ferric ions was larger for smaller water cuts where the ratio between the metal surface exposed to the brine and the brine volume was lower.

It is worth mentioning that the change of the IFT towards lower values during the flow experiments with the carbon steel bottom surface may have favored the entrainment of the water phase. This is due to the formation of droplets of smaller size when the water phase is disrupted by the inertial and viscous forces of the turbulent oil flow [33]. These smaller droplets are easier to suspend against gravity by the turbulent dispersive forces of the continuous phase flow preventing their segregation.

3.3. Hydrodynamics of the annular flume flow and its impact on water entrainment in oil-water flow

The discussion in this section is focused on characterization of the complex hydrodynamics of the annular flume flow, by using relatively simple assumptions, in order to test criteria meant to assess the stability of fully dispersed oil-water flow in pipes. This should lead to deeper insights when it comes to the experimental behavior described in the previous section.

3.3.1. Turbulent single-phase flow in the annular flume

Fig. 7 shows a schematic representation of the annular flume geometry and the tangential velocity profile at the mid radius (R) in single-phase turbulent flow, produced by the rotation of the top wall. The shear stress at the bottom wall, which is where the entrainment of the water phase occurs, varies as a function of the radial direction as shown in the example of Fig. 8 from the numerical modeling performed by Maa [34]. This is due to the corners of the rectangular section of the annular flume, the tangential velocity gradient, and also the existence of secondary cross flow as indicated in Fig. 2b and c. In general, the bottom wall shear stress (τ_{wb}) presents a main tangential component and also a minor radial component that can range from 10% to 20% of the wall shear stress modulus, depending on the magnitude of the cross flow velocity (r direction) relative to the main tangential velocity (t direction) [30,34,35]. Due to this reason, the average wall shear stress can be reasonably estimated considering only the effect of the tangential velocity of the flume flow, neglecting the cross flow velocity, as:

$$\bar{\tau_{wb}} \cong \frac{1}{2}\rho f_{fl} U_{fl}^2 \tag{4}$$

where f_{fl} is the Fanning friction factor, ρ is the density of the fluid, and U_{fl} is the mean tangential velocity calculated in Eq. (2).

If it is assumed that the hydrodynamic boundary layer at the bottom wall behaves similarly to that of turbulent Couette flow, the friction factor can be calculated as [36]:

$$\sqrt{\frac{2}{f_{fl}}} = 2.43\ln\left(Re_{fl}\sqrt{\frac{f_{fl}}{2}}\right) + 5 \tag{5}$$

Eq. (5) can be approximated with less than 10% absolute error in the range $400 < Re_{fl} < 100{,}000$ by using the explicit Blasius type equation:

$$f_{fl} = 0.033 Re_{fl}^{-0.2} \tag{6}$$

where Re_{fl} is the Reynolds number of the flume:

$$Re_{fl} = \frac{\rho H U_{fl}}{2\mu} \tag{7}$$

where μ is the dynamic viscosity of the fluid. It is worth indicating that the laminar/turbulent transition in Couette flow is given at Reynolds numbers from 320 to 360 [37,38].

Fig. 9 shows measured values of average bottom wall shear stress [35,39] as well as numerical predictions [35,40] as a function of the rotation speed of the top wall in single-phase turbulent flow of water in annular flumes with different dimensions. The simplified calculation using Eq. (4) shows fairly good agreement with the experimental data, and is also close to the numerical predictions.

Another very important parameter to characterize the annular flume flow is the torque input on the rotating top plate, which is equivalent to:

$$T = \int r \times \tau_{wt}(r) dA = \int r \times \tau_{wb}(r) dA + \int r \times \tau_{wo}(z) dA + \int r \times \tau_{wi}(z) dA \tag{8}$$

where $\tau_{wt}(r)$ is the shear stress at the rotating top wall, and $\tau_{wo}(z)$ and $\tau_{wi}(z)$ are the shear stresses at the outer and the inner walls, respectively. Eq. (8) does not consider the torque at the slits between the rotating plate and the inner and outer walls of the flume, which is estimated to be less than 10% of the total torque value. The torque can be also expressed as a function of average wall shear stresses as:

$$T \cong R\bar{\tau_{wt}}A_a \cong R\bar{\tau_{wb}}A_a + R_o\bar{\tau_{wo}}A_o + R_i\bar{\tau_{wi}}A_i \tag{9}$$

where

$$A_a = \pi(R_o^2 - R_i^2); \tag{10}$$

$$A_o = 2\pi R_o H; \tag{11}$$

$$A_i = 2\pi R_i H \tag{12}$$

Table 2
Oil-water interfacial tension (σ) measurements before and after flow experiments.

Bottom surface material	σ (N/m) × 10^3	
	Before experiments	After experiments
Carbon steel	41.5 ± 1	26.8–34.7
Stainless steel		37.5–38.9
PET		35.5–39.6

Table 3
Oil-water interfacial tension (σ) and concentration of dissolved iron ions in the water phase for different water cuts (WC) tested with the carbon steel bottom surface.

WC (%)	σ (N/m) × 10^3	Dissolved iron ions (ppm)
2.5	28.5 ± 0.2	4.8 ± 1
5	26.8 ± 0.1	19 ± 4
7.5	27.1 ± 0.1	20 ± 4
10	34.7 ± 0.3	0.5 ± 0.2

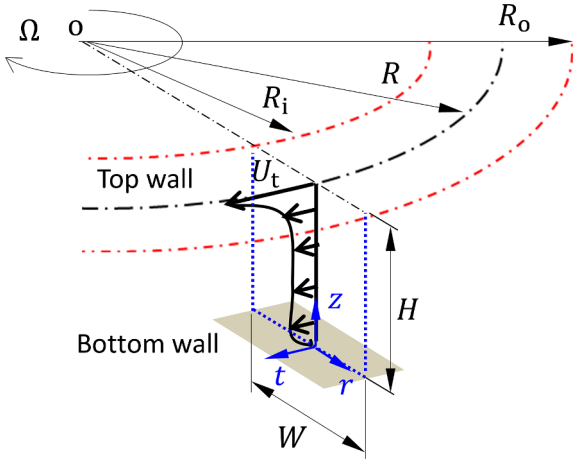

Fig. 7. Schematic representation of the annular flume geometry and the tangential velocity profile in turbulent flow at the mid radius.

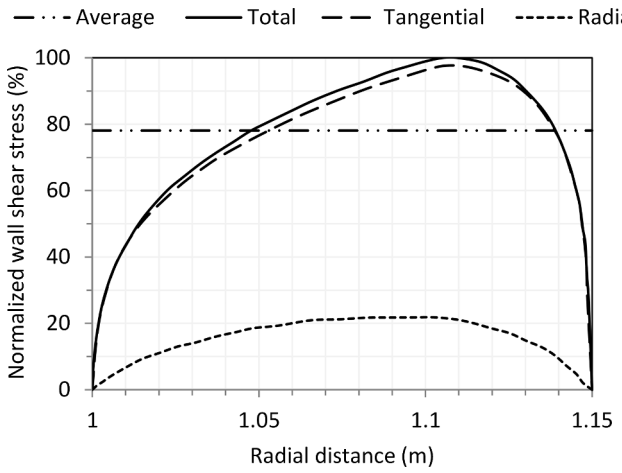

Fig. 8. Normalized bottom wall shear stress in function of the radial distance in an annular flume with R_i = 1 m, R_o = 1.15 m and H = 0.1 m in single-phase turbulent flow of water at Ω = 8 rpm. Average wall shear stress is 0.38 Pa [34].

Eq. (9) can be written only as a function of the bottom wall shear stress:

$$T \cong \bar{\tau}_{wb}(RA_a + C_o R_o A_o + C_i R_i A_i) \quad (13)$$

where C_o and C_i are constants that relate the bottom wall shear stress with the wall shear stresses at the outer and inner cylinders, respectively. The average value of the constants C_o and C_i was determined as 2.5 and 0.5, respectively, from the experimental data of Graham et al. [35]. Graham et al. also made numerical predictions that lead to average values of C_o and C_i of 2.3 and 0.6, respectively. In this work, the constants C_o = 2.5 and C_i = 0.5 are adopted for Eq. (13). Fig. 10 shows measured values and numerical predictions [35] of torque at the rotating top wall of an annular flume as a function of the rotation speed in single-phase turbulent flow of water. The torque calculated using Eq.

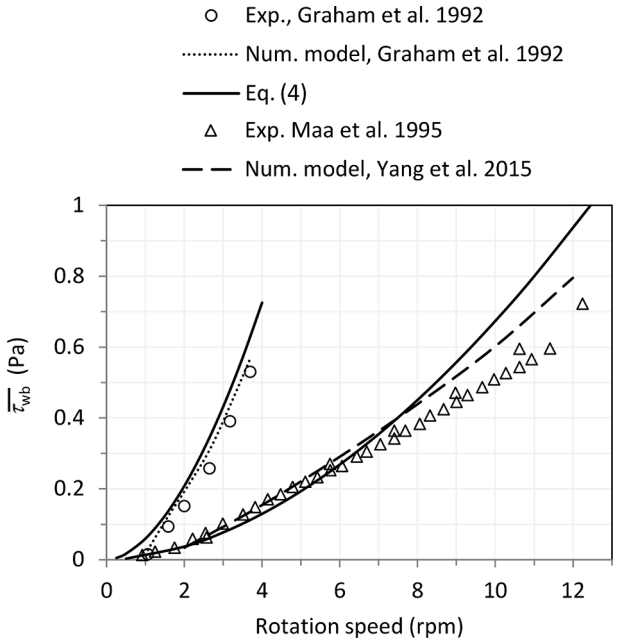

Fig. 9. Measured and calculated average bottom wall shear stress as a function of rotation speed in annular flumes with: R_i = 2.6 m, R_o = 3 m and H = 0.1 m (Graham et al. [35]); and R_i = 1 m, R_o = 1.15 m and H = 0.1 m (Maa et al. [39]). Single-phase turbulent flow of water.

(13) agrees well with the available experimental data and predictions from numerical modeling. It must be mentioned that Graham et al. used a relatively large width to height ratio (W/H) of 4 compared to the value of 1.55 used in this work; therefore, the adopted values for the constants C_o and C_i may not be as accurate in this case. Unfortunately, as per the knowledge of the authors, there is no data available in the literature for lower W/H ratios to check the values of C_o and C_i.

3.3.2. Comparison of the phase wetting data with available hydrodynamic criteria

Hydrodynamic criteria, previously developed to evaluate the stability of fully dispersed oil-water flow in pipes, will be used here to assess the same in oil-water flow in the annular flume. These criteria

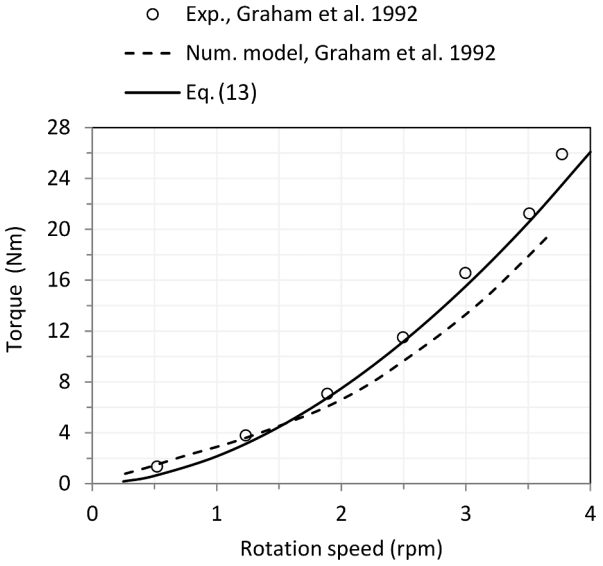

Fig. 10. Measured and calculated torque at the rotating top wall as a function of rotation speed in an annular flume with: R_i = 2.6 m, R_o = 3 m and H = 0.1 m (Graham et al. [35]). Single-phase turbulent flow of water.

assume that the flow is already fully dispersed and assess its stability against the segregation of the dispersed phase. Moreover, the dispersed flow of oil and water is considered as a homogeneous mixture. Brauner [14] proposed that the transition to dispersed flow pattern takes place when the continuous phase turbulence is sufficiently intense to disrupt the dispersed phase into droplets smaller than the critical size (d_{crit}) with the transitional criterion:

$$d_{max} \leq d_{crit} \tag{14}$$

The key proviso in this scenario is that the continuous phase flow is turbulent. In the case of the annular flume flow, this is assumed for$Re_{fl} > 360$. The critical droplet diameter is estimated as:

$$d_{crit} = Min(d_{cb}, d_{c\sigma}) \tag{15}$$

where d_{cb} is the maximum droplet size above which droplets will migrate to the bottom pipe wall due to gravity:

$$d_{cb} = \frac{3}{8}\frac{\rho_c f U_c^2}{(\rho_d - \rho_c) g \cos\beta} \tag{16}$$

where f is the Fanning friction factor of the pipe, g is the gravitational constant, β is the pipe inclination angle from the horizontal, ρ_c and ρ_d are the densities of the continuous (oil) and the dispersed (water) phase, respectively; and U_c is the mean velocity of the continuous phase. Adapting Eq. (16) to the annular flume flow leads to:

$$d_{cb} = \frac{3}{8}\frac{\rho_c f_{fl} U_{fl}^2}{(\rho_d - \rho_c) g} \tag{17}$$

It must be mentioned that Eq. (16) is derived from the balance between the gravity force and the drag force produced by the average vertical turbulent velocity fluctuations of the oil flow on a dispersed water droplet. In the case of the annular flume, there are two net cross flow components acting close to the center of the bottom wall, one in the radial direction (r) moving towards the center of the annulus, and the other in the vertical or axial direction (z) moving towards the top of the conduit. The first one is lower than 10% of the average tangential velocity of the top wall (U_t) [30,34], and its convective effect does not directly contribute to lift water droplets, as is the case with the tangential flow component. However, the second cross flow component appears to directly add to the drag force of the oil phase against gravity. The rms value of vertical turbulent fluctuations of the oil flow near the bottom wall is considered to be $\cong U_{fl}\sqrt{f_{fl}/2}$, which represents about 2% of U_t in the present case study. In general, the average value of the vertical flow component is very small at the center of the cross-section of the conduit, i.e., < 1% of U_t [30,34], and is even smaller close to the bottom wall. Therefore, the assumption of only turbulent forces against gravity behind Eq. (17) can still hold true.

The parameter $d_{c\sigma}$ is the droplet diameter above which droplets deform excessively from their spherical shape mainly due to gravity, and turbulent flow forces are no longer effective to fully disperse droplets and impede their contact with the bottom pipe wall:

$$d_{c\sigma} = \left[\frac{0.4\sigma}{(\rho_d - \rho_c) g \cos\beta^{'}}\right]^{1/2} \tag{18}$$

where σ is the oil-water interfacial tension, and $\beta^{'} = |\beta|$ when $|\beta|$ is below 45 degrees. In the case of the horizontal annular flume, the term $\cos\beta^{'}$ is equal to 1.

The maximum droplet size of the dispersed phase can be calculated as [33]:

$$d_{max,o} = 0.725\left(\frac{\sigma}{\rho_c}\right)^{3/5} \epsilon^{-2/5} \tag{19}$$

where ϵ is the mean energy dissipation rate of the continuous phase flow. Since Eq. (19) is only valid for dilute dispersions, to account for the effect of the volumetric fraction of dispersed phase (water cut) $d_{max,o}$ is modified by the factor suggested by Mlynek and Resnik [41]. Then, the maximum droplet size is:

$$d_{max} = d_{max,o}(1 + 5.4\varepsilon_d) \tag{20}$$

The mean energy dissipation rate in the annular flume flow can be expressed as:

$$\epsilon_{fl} = \frac{T\Omega}{HA_a\rho_c(1 - \varepsilon_d)} \tag{21}$$

where ε_d is the volumetric fraction of dispersed phase that in this case is equivalent to the water cut. The calculation of the parameters d_{cb} and ϵ_{fl} require the estimation of the friction factor f_{fl} in Eq. (6). This friction factor, in the case of homogeneous dispersed oil-water flow, is calculated with the Reynolds number in Eq. (7) using the mixture density:

$$\rho_m = \rho_c(1 - \varepsilon_d) + \rho_d\varepsilon_d \tag{22}$$

The mixture viscosity is approximated to the viscosity of the continuous phase (oil) $\mu_m \cong \mu_c$. It is noteworthy that the largest turbulence, and correspondingly the largest dissipated energy in the continuous phase flow, occurs close to the top rotating wall where the wall shear stress is larger than the bottom wall shear stress by a factor $(A_a + C_oA_oR_o/R + C_iR_i/R)A_a^{-1}$ (see Eqs. (9) and (13)). For the actual geometry of the studied annulus this gives about 3.6. Consequently, droplet breakup is supposed to be stronger close to the top wall than at the side and bottom walls of the conduit. This feature differs from pipe flow where the wall shear stress is considered to be similar around the pipe circumference. Therefore, the translation of experimental results relating to the criteria in Eqs. (14) and (15) from the annulus to the pipe is not straightforward in terms of mean flow velocities. This requires other strategies, such as matching produced droplet sizes, which is most reasonable given the droplet deformation criterion ($d_{c\sigma} \leq d_{max}$). However, a more comprehensive analysis is needed for the droplet buoyancy criterion ($d_{cb} \leq d_{max}$), in which the produced droplet sizes and the turbulent lift forces close to the wall are related in different ways.

It must be mentioned that in oil-water stratified flow, the water phase is driven towards the inner wall of the flume due to the secondary cross flow of the top oil layer, as shown by de Dood [27]. Therefore, water entrainment is expected to occur first at the outer area of the bottom wall, where the wall shear stress is at a maximum, and finish at its inner area where wall shear stress decreases. From this point of view, the use of an average friction parameter to assess water entrainment and fully dispersed flow (e.g., Eq. (17)) may not be as accurate.

Given that the adapted set of criteria provided by Brauner [14] attempts to define the conditions at which water droplets are not effectively suspended by the oil flow and migrate towards the conduit bottom wall making contact and causing segregation, its use is mostly suitable for hydrophilic surfaces where droplets actually stick and spread leading to water wetting [10]. Fig. 11 shows Brauner's criteria on the phase wetting map obtained for the hydrophilic carbon steel bottom wall. To account for the variation of the oil-water interfacial tension observed in the experiments, the theoretical dispersed flow bounds described by Eqs. (14) and (15) were calculated for the highest (Fig. 11 top) and the lowest (Fig. 11 bottom) measured interfacial tension values of 0.04 N/m and 0.027 N/m, respectively. Both bounds described by the critical droplet sizes d_{cb} and $d_{c\sigma}$, which are close to each other for this particular case study, seem to describe somewhat well the transition from water wet to oil wet regimes for the available experimental data when the water cut is larger than 2.5%. In particular, the droplet deformation criterion ($d_{c\sigma} \leq d_{max}$) correlates better with the experimental data.

It is worth restating that the used criteria assume the transition from dispersed flow to segregated flow, and the performed experiments switched from segregated flow to dispersed flow. In this case, other mechanisms such as the shearing of thin segregated water layers by the oil flow as well as the interaction of settling water droplets with the layers may play an important role, but are not considered by Brauner's criteria as discussed elsewhere [10]. Nevertheless, the present results

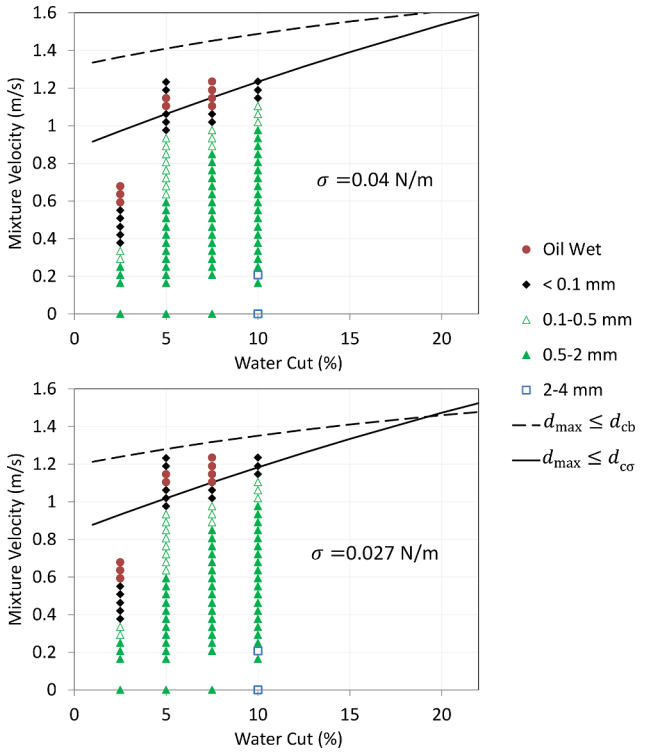

Fig. 11. Comparison of dispersed flow criteria with maps of phase wetting regime and time-averaged water layer thickness for the carbon steel bottom plate in the annular flume oil-water flow. Top: bounds were calculated using $\sigma = 0.04$ N/m; Bottom: bounds were calculated using $\sigma = 0.027$ N/m.

are promising since the transition to fully dispersed flow, and eventually full oil wet regime, might be characterized well enough for practical purposes by Eq. (15) when the bottom surface of the conduit is hydrophilic, as in the case of carbon steel in contact with oil-water systems that do not alter wettability. In the case of hydrophobic bottom surfaces (i.e., PET and to lesser degree stainless steel), the transition to fully dispersed flow and full oil wet regime is given at much lower flow velocities than predicted by Eq. (15) (Figs. 5, 6 and 11). The same behavior was observed in pipe flow where droplet accumulation at the pipe bottom sufficient to reach a critical concentration for major droplet coalescence (e.g., the phase inversion point) was suggested as the criterion to define the fully dispersed flow bound in a hydrophobic pipe [10]. Unfortunately, the annular flume flow presents main and secondary flow currents that vary across its cross-section. This makes the implementation of transport (advection-diffusion) models to describe the distribution of dispersed droplets [42] very difficult and the aid of numerical methods is required. It is important to note that the existence of vertical convective currents in the annulus, which are of the order of the settling velocities of dispersed droplets, greatly alters droplet concentration gradients. Therefore, direct comparison of droplet concentration distributions to the ones in a pipe is impossible, as also discussed elsewhere [28].

3.4. General remarks

It has been shown that the wettability of the bottom wall of the used annular flume can significantly influence the phase wetting regime (oil wet or water wet) and the onset of water-in-oil dispersion in oil-dominated two-phase oil-water flow. The onset of fully dispersed flow (oil wetting) occurs at larger mixture velocities for hydrophilic bottom plates (e.g., carbon steel) than in hydrophobic bottom plates (e.g., PET and stainless steel), similar to what was observed in pipes [10]. These results are very promising from the point of view of the potential use of this type of small scale device to qualify the effect of a given crude oil-water system on the phase wetting behavior of carbon steel or any other, similar or otherwise, pipe material of interest. The qualitative analysis can be performed by comparing the behavior of oil-water mixtures using a carbon steel bottom surface, which may behave as hydrophilic or hydrophobic depending on the used oil and water, with the response of the same oil-water system using a known hydrophobic bottom surface (e.g., an inert polymer). Actually, the theoretical assessment presented above (Eqs. (14) and (15)) can directly give an idea of the expected water-wet-to-oil-wet transition on hydrophilic surfaces, provided that the properties of the oil and water are known. Therefore, phase wetting experiments can be performed directly with carbon steel bottom surfaces and then it can be concluded if the used crude oil-water mixture alters or not the wettability of carbon steel and its dynamic phase wetting behavior, by comparing the theoretical and experimental phase wetting transition bounds.

A more complete picture of the behavior of the tested oil-water flow in the annulus can definitely be obtained if the concentration of dispersed water droplets in the conduit cross-section is well predicted. In this way, the phase wetting transition measured for hydrophobic bottom surfaces might be related to the attainment of critical droplet concentrations, e.g., at the bottom of the flume. These concentrations can be compared to the inversion point of the oil-water mixture or other critical droplet concentration, where droplet coalescence is assumed as inevitable [2,10], giving a very important insight for field applications. In relation to this deduction, it is planned to continue the work on the implementation of a numerical model for the continuous phase flow, coupled with a transport model for the characterization of the dispersed phase fraction, in an attempt to describe the complexity of the dispersed oil-water flow in the annulus. As discussed above, direct use of the critical flow velocities for full water entrainment found in the annulus is not possible for field applications due to the intrinsic differences between the annulus and the pipe flow. However, a good understanding of multiphase flow in the annular flume would allow more accurate description of the observed experimental behavior, based on relevant criteria (e.g., droplet suspension by turbulent forces, critical droplet concentration, etc.), which can then be translated to pipe flow via modeling.

4. Conclusions

- The wettability of the bottom surface of the annular flume greatly affects the phase wetting regime (oil-wet or water-wet) and the onset of fully dispersed water-in-oil flow. For example, the onset of fully dispersed flow occurs at significantly larger mixture velocities in the presence of hydrophilic surfaces (e.g., carbon steel) rather than with hydrophobic surfaces (e.g., PET and stainless steel). This behavior is similar to what was observed in oil-water flow in pipes with different wettability.
- Given the significant differences observed between the experimental behavior of hydrophilic and hydrophobic surfaces, the small-scale annular flume can be successfully used for the qualitative characterization of the effect of the chemical composition of crude oil-water systems on the wettability and phase wetting behavior of carbon steel or any other pipe material of interest in oil-water flow.
- Basic analysis of the annular flume flow was performed in order to adapt Brauner's criteria, which were developed to predict critical velocities for fully dispersed flow in pipes. It was found that these criteria agree somewhat well with the experimental water-wet-to-oil-wet transition in the annular flume flow with hydrophilic bottom surfaces; particularly, for water cuts larger than 2.5%.
- Direct use of the critical flow velocities for full water entrainment found in the annulus is not possible for field applications due to the intrinsic differences between the annulus and the pipe flow. Good knowledge of multiphase flow in the annular flume would allow the possibility to accurately describe the experimental behavior based on relevant criteria that can be subsequently translated to pipes by means of modeling.

Acknowledgements

This work was funded by Ohio University's Institute for Corrosion and Multiphase Technology (ICMT) and Honors Tutorial College. We are grateful to Dr. Bert Pots for providing helpful comments during preparation of this manuscript. The authors also want to acknowledge the laboratory engineers Albert Schubert and Cody Shafer and technician Alexis Barxias, at the ICMT, for their assistance and constructive support.

References

[1] M.B. Kermani, A. Morshed, Carbon dioxide corrosion in oil and gas production - a compendium, Corrosion 59 (2003) 659–683.
[2] B.F.M. Pots, J.F. Hollenberg, E.L.J.A. Hendriksen, What are the real influences of flow on corrosion? NACE Corrosion 2006, NACE, Houston, TX, 2006 Paper 6591.
[3] S.N. Smith, M.W. Joosten, Corrosion of carbon steel by H_2S in CO_2 containing oilfield environments, NACE Corrosion 2006, NACE, Houston, TX, 2006 Paper 6115.
[4] J. Cai, C. Li, X. Tang, F. Ayello, S. Richter, S. Nesic, Experimental study of water wetting in oil–water two phase flow—horizontal flow of model oil, Chem. Eng. Sci. 73 (2012) 334–344.
[5] U. Lotz, L.V. Bodegom, C. Ouwehand, The effect of type of oil or gas condensate on carbonic acid corrosion, Corrosion 47 (1991) 636–645.
[6] F. Ayello, C. Li, X. Tang, J. Cai, S. Nesic, C.I.T. Cruz, J.N. Al-Khamis, Determination of phase wetting in oil-water pipe flows, NACE Corrosion 2008, NACE International, Houston, TX, 2008 Paper 8566.
[7] K.E. Kee, S. Richter, M. Babic, S. Nešić, Experimental study of oil-water flow patterns in a large diameter flow loop—the effect on water wetting and corrosion, Corrosion 72 (2016) 569–582.
[8] L.D. Paolinelli, J. Yao, A. Rashedi, Phase wetting detection and water layer thickness characterization in two-phase oil-water flow using high frequency impedance measurements, J. Petrol. Sci. Eng. 157 (2017) 671–679.
[9] X. Tang, Effect of Surface State on Water Wetting and Carbon Dioxide Corrosion in Oil-water Two-phase Flow, PhD thesis Department of Chemical and Biomolecular Engineering, Ohio University, Athens, OH, 2011, p. 206.
[10] L.D. Paolinelli, A. Rashedi, J. Yao, M. Singer, Study of water wetting and water layer thickness in oil-water flow in horizontal pipes with different wettability, Chem. Eng. Sci. 183 (2018) 200–214.
[11] H. Pouraria, J.K. Seo, J.K. Paik, A numerical study on water wetting associated with the internal corrosion of oil pipelines, Ocean Eng. 122 (2016) 105–117.
[12] D.T. Tsahalis, Conditions for the entrainment of settled water in crude oil and product pipelines, 83rd National Meeting of the AIChE, AIChE, Houston, TX, 1977, p. 50.
[13] M. Wicks, J.P. Fraser, Entrainment of water by flowing oil, Mater. Perform. 14 (1975) 9–12.
[14] N. Brauner, The prediction of dispersed flows boundaries in liquid–liquid and gas–liquid systems, Int. J. Multiph. Flow 27 (2001) 885–910.
[15] J.L. Trallero, Oil-Water Flow Patterns in Horizontal Pipes, PhD thesis University of Tulsa, Tulsa, OK, 1995, p. 176.
[16] NACE, SP0208-2008, Internal Corrosion Direct Assessment Methodology for Liquid Petroleum Pipelines, NACE, Houston TX, 2008, p. 32.
[17] D. Barnea, A unified model for predicting flow-pattern transitions for the whole range of pipe inclinations, Int. J. Multiph. Flow 13 (1987) 1–12.
[18] P. Angeli, G.F. Hewitt, Flow structure in horizontal oil–water flow, Int. J. Multiph. Flow 26 (2000) 1117–1140.
[19] M.E. Charles, G.W. Govier, G.W. Hodgson, The horizontal pipeline flow of equal density oil-water mixtures, Canad. J. Chem. Eng. 39 (1961) 27–36.
[20] D. Hasson, V. Mann, A. Nir, Annular flow of two immiscible liquids I. Mechanisms, Canad. J. Chem. Eng. 48 (1970) 514–520.
[21] M. Nädler, D. Mewes, Flow induced emulsification in the flow of two immiscible liquids in horizontal pipes, Int. J. Multiph. Flow 23 (1997) 55–68.
[22] T.K. Mandal, D.P. Chakrabarti, G. Das, Oil-water flow through different diameter pipes: similarities and dissimilarities, Chem. Eng. Res. Des. 85 (2007) 1123–1128.
[23] G. Aspenes, L.E. Dieker, Z.M. Aman, S. Høiland, A.K. Sum, C.A. Koh, E.D. Sloan, Adhesion force between cyclopentane hydrates and solid surface materials, J. Colloid Interface Sci. 343 (2010) 529–536.
[24] F. Ayello, W. Robbins, S. Richter, S. Nesic, Model compound study of the mitigative effect of crude oil on pipeline corrosion, Corrosion 69 (2013) 286–296.
[25] S. Richter, M. Babic, X. Tang, W. Robbins, S. Nesic, Categorization of Crude Oils Based on Their Ability to Inhibit Corrosion and Alter the Steel Wettability, NACE Corrosion 2014, NACE, Houston, TX, 2014 Paper 4247.
[26] C. Li, Effect of Corrosion Inhibitor on Water Wetting and Carbon Dioxide Corrosion in Oil-Water Two-Phase Flow, PhD thesis Department of Chemical and Biomolecular Engineering, Ohio University, Athens OH, 2009, p. 198.
[27] M.J.A. de Dood, Oil/water Flow in a Carousel, MSc thesis, Technical Physics, University of Amsterdam, Amsterdam, 1997, p. 30.
[28] P.H. Ligthart, Water drop-out and water entrainment in crude oil pipelines, MSc thesis Laboratory for Aero and Hydrodynamics Delft University of Technology, Delft, 1997, p. 86.
[29] C. Li, S. Richter, S. Nešić, How do inhibitors mitigate corrosion in oil-water two-phase flow beyond lowering the corrosion rate? Corrosion 70 (2014) 958–966.
[30] Z. Yang, A. Baptista, J. Darland, Numerical modeling of flow characteristics in a rotating annular flume, Dyn. Atmos. Oceans 31 (2000) 271–294.
[31] S. Srinivasan, G.H. McKinley, R.E. Cohen, Assessing the accuracy of contact angle measurements for sessile drops on liquid-repellent surfaces, Langmuir 27 (2011) 13582–13589.
[32] J.L. Trallero, C. Sarica, J.P. Brill, A study of oil-water flow patterns in horizontal pipes SPE production & facilities, 12 (1997) 165–172.
[33] J.O. Hinze, Fundamentals of the hydrodynamic mechanism of splitting in dispersion processes, AIChE J. 1 (1955) 289–295.
[34] J.P.-Y. Maa, VIMS Sea Carousel: Its Hydrodynamic Characteristics, in: A.J. Mehta (Ed.), Nearshore and Estuarine Cohesive Sediment Transport, American Geophysical Union, Washington DC, 1993, pp. 265–279.
[35] D.I. Graham, P.W. James, T.E.R. Jones, J.M. Davies, E.A. Delo, Measurement and prediction of surface shear stress in annular flume, J. Hydraul. Eng. 118 (1992) 1270–1286.
[36] S. Pirozzoli, M. Bernardini, P. Orlandi, Turbulence statistics in Couette flow at high Reynolds number, J. Fluid Mech. 758 (2014) 327–343.
[37] S. Bottin, H. Chaté, Statistical analysis of the transition to turbulence in plane Couette flow, Eur. Phys. J. B – Condens. Matter Complex Syst. 6 (1998) 143–155.
[38] N. Tillmark, P.H. Alfredsson, Experiments on transition in plane Couette flow, J. Fluid Mech. 235 (1992) 89–102.
[39] J.P.Y. Maa, C.H. Lee, F.J. Chen, Bed shear stress measurements for vims Sea Carousel, Mar. Geol. 129 (1995) 129–136.
[40] S.-H. Yang, I.-T. Im, K.-N. Hwang, Y.-S. Cho, H.-R. Ryu, A numerical study on optimal rotation ratio and bottom shear stress in the counter-rotation mode of an annular flume, J. Hydro-environ. Res. 9 (2015) 473–481.
[41] Y. Mlynek, W. Resnick, Drop sizes in an agitated liquid-liquid system, AIChE J. 18 (1972) 122–127.
[42] A.J. Karabelas, Vertical distribution of dilute suspensions in turbulent pipe flow, AIChE J. 23 (1977) 426–434.